A&A manuscript no.
(will be inserted by hand later)

Your thesaurus codes are:
09.13.2, 11.09.4, 11.14.1, 11.19.3, 13.19.1

ASTRONOMY
AND
ASTROPHYSICS
1.2.2008

Dense gas in nearby galaxies

XI. H_2CO and CH_3OH: Molecular abundances and physical conditions

S. Hüttemeister[1,2], R. Mauersberger[3,4], C. Henkel[3]

[1] Radioastronomisches Institut der Universität Bonn, Auf dem Hügel 71, D - 53121 Bonn, Germany
[2] Harvard-Smithsonian Center for Astrophysics, 60 Garden Street, Cambridge, MA 02138, U.S.A
[3] Max-Planck-Institut für Radioastronomie, Auf dem Hügel 69, D - 53121 Bonn, Germany
[4] Steward Observatory, The University of Arizona, Tucson, AZ 85721, U.S.A.

received 7 November 1996; accepted 29 April 1997

Abstract. Multilevel observations of formaldehyde (H_2CO) and methanol (CH_3OH) toward the nearby spiral galaxies NGC 253, Maffei 2, IC342, M 82 and NGC 6946 are presented. H_2CO was detected in all galaxies (tentatively in NGC 6946). CH_3OH was detected in all objects with the notable exception of M 82.

H_2CO line intensity ratios point out differences in gas density both between galaxies and within the central regions of individual objects. Model calculations show that the bulk of the gas emitting H_2CO in NGC 253 is at a density of $\sim 10^4\,\mathrm{cm}^{-3}$, while the H_2CO lines in M 82 and IC 342 trace two different, spatially separated gas components with densities of $\leq 10^4\,\mathrm{cm}^{-3}$ and $\sim 10^6\,\mathrm{cm}^{-3}$. The south-western molecular hotspot in M 82 and the center of IC 342 are the regions with the highest density.

Methanol is subthermally excited in all galaxies, with the lowest excitation temperatures found in IC 342. The CH_3OH abundance in NGC 253 and the non-starburst nuclei of IC 342 and Maffei 2 are comparable. A map of the $3_k - 2_k$ lines in NGC 253 shows that CH_3OH traces clumpy structures better than other molecules requiring high gas density to be excited. CH_3OH toward M 82 is at least an order of magnitude less abundant than in otherwise comparable galaxies. This confirms the existence of global chemical differences, and thus very large scale variations in the state of the molecular gas phase, even between galaxies commonly classified as starburst nuclei.

Key words: ISM: molecules – galaxies: ISM – galaxies: nuclei – galaxies: starburst – radio lines: galaxies

Send offprint requests to: S. Hüttemeister, RAIUB

1. Introduction

The central regions of galaxies, including our own, are characterized by a unique population of molecular clouds, both denser and warmer than typical disk clouds. In galaxies undergoing a nuclear starburst, these clouds are subject to turbulence and intense UV radiation, as well as shocks, due to both a steep gravitational potential and the formation and death of young massive stars. They form a distinct type of interstellar molecular environment, different from Galactic dark clouds and the surroundings of H II regions. Galactic center clouds are a rich source of molecular emission; ~ 25 molecular species have been discovered in the nuclear regions of external galaxies.

Formaldehyde and methanol are both useful tracers of the dense interstellar gas phase. Their molecular structure is more complicated than that of HCN or CS, the "classical" tracers of dense gas. This leads to a greater wealth of transitions which can be observed in the millimeter wavelength range, providing a powerful tool to understand the physical and chemical conditions of the gas associated with starbursts.

The first *formaldehyde* transitions detected in external galaxies were K-doublet ortho transitions in the centimeter wavelength range ($1_{10} - 1_{11}$ at 6 cm and $2_{11} - 2_{12}$ at 2 cm; Gardner & Whiteoak 1974, 1976, 1979, Whiteoak & Gardner 1976, Cohen et al. 1979, Graham et al. 1978, Seaquist & Bell 1990, Baan & Goss 1992). Galaxies where these lines have been detected include NGC 253, NGC 4945, M 82, Centaurus A, NGC 3628, M 31 and the LMC. Recently, the $2_{11} - 2_{12}$ transition has been detected toward the Einstein Ring gravitational lens system B0218+357 at a redshift of $z = 0.68$ (Menten & Reid 1996). In all the above sources the lines are observed in absorption; with $T_{\mathrm{ex}} < 2.7\,\mathrm{K}$, they can absorb even the microwave background. The $1_{10} - 1_{11}$ line emission was first observed toward Arp 220 (Baan et al. 1986). Detections in

nine other galaxies and an interferometric map of Arp 220 (Baan et al. 1993, Baan & Haschick 1995) followed. These lines are interpreted as H_2CO megamasers.

There are less observations of the rotational transitions at millimeter wavelengths, even though these transitions are sensitive tracers of cloud temperature and density. The $3_{03} - 2_{02}$ para transition was discovered in M 82 (Baan et al. 1990), the $3_{21} - 2_{20}$ para line was observed in NGC 253 (Petuchowski & Bennett 1992), and the $3_{12} - 2_{11}$ ortho transition was detected in the LMC by Johansson et al. (1994) and tentatively in the southern galaxy NGC 4945 (Mauersberger et al. 1996b).

The first successful observation of extragalactic *methanol* (CH_3OH) was reported in 1987 by Henkel et al.. They detected a superposition of four $2_k - 1_k$ transitions at 96 GHz in NGC 253, IC 342 and (tentatively) NGC 6946. This group of transitions requires only low excitation and all four components are among the strongest methanol lines observed in Galactic sources. The same group of transitions was detected in the southern starburst galaxy NGC 4945 (Henkel et al. 1990). The $0_0 - 1_{-1}E$ transition was seen toward NGC 253 by Henkel et al. (1993). Methanol masers, very common in the Galaxy, are also detected toward the Large Magellanic Cloud at 6.6 GHz (Sinclair et al. 1992, Ellingsen et al. 1994). Here, we report observations of six H_2CO and seven CH_3OH rotational transitions toward five galaxies, thus considerably expanding the existing database.

Table 1. Summary of the observed transitions. For H_2CO, *o* and *p* denote ortho and para transitions.

Line	Frequency GHz	$E_u^{a)}$ K	θ $''$
H_2CO			
$2_{12} - 1_{11}$ *o*	140.840	17	16
$2_{02} - 1_{01}$ *p*	145.603	10	16
$2_{11} - 1_{10}$ *o*	150.498	23	16
$3_{13} - 2_{12}$ *o*	211.211	32	12
$3_{03} - 2_{02}$ *p*	218.222	21	12
$3_{12} - 2_{11}$ *o*	225.698	33	12
CH_3OH			
$5_{-1} - 4_0$E	84.521	32	27
$2_k - 1_k^{b)}$	96.741	5–20	27
$3_1 - 2_1A^+$	143.866	28	16
$3_k - 2_k^{c)}$	145.103	12–51	16
$7_1 - 8_0$E	220.07	88	12
$8_{-1} - 7_0$E	229.75	81	12
$3_{-2} - 4_{-1}$E	230.027	32	12

a) Energy of the upper level; for E-type methanol, the values refer to the 1_1-level, 6.9 K above ground.
b) Lines contributing to the $2_k - 1_k$ group: $2_{-1} - 1_{-1}E$ (5 K), $2_0 - 1_0A^+$ (6 K), $2_0 - 1_0E$ (12 K), $2_1 - 1_1E$ (20 K)
c) Lines contributing to the $3_k - 2_k$ group: $3_0 - 2_0E$ (19 K), $3_{-1} - 2_{-1}E$ (12 K), $3_0 - 2_0A^+$ (14 K), $3_2 - 2_2A^-$ (51 K), $3_2 - 2_2E$ (28 K), $3_{-2} - 2_{-2}E$ (32 K), $3_1 - 2_1E$ (27 K), $3_2 - 2_2A^+$ (51 K)

2. Observations

All observations were carried out with the IRAM 30-m antenna. The measurements were made with SIS receivers tuned to a single sideband with image sideband rejections of typically 7 dB. An error in the determination of the sideband rejection of ±1 dB would result in an additional calibration uncertainty of ±5%. The temperature scale used throughout this paper is main-beam brightness temperature (T_{MB}). System temperatures were between 540 K and 580 K T_{MB} in the 3 mm wavelength range, between 600 K and 900 T_{MB} at 2 mm wavelength and between 1200 K and 1800 K T_{MB} at 1.3 mm. All transitions were observed with either a 512 × 1 MHz filterbank or a 864 channel acousto-optical spectrometer (AOS) with a total bandwidth of 500 MHz.

The observed transitions, including their designations, frequencies and energies above ground (Mangum & Wootten 1993, Anderson et al. 1990), and the beamwidth of the telescope, are summarized in Table 1.

For broad lines encountered in external galaxies, it is not only the system noise that determines the accuracy of line intensies and ratios, but also the flatness of the spectrometer bandbass, which is affected by the stability of the weather and the electronic components. We used a wobbling secondary mirror, switching with a frequency of 0.5 Hz between the source and two reference positions placed symmetrically at $4'$ offset in azimuth. The backends are of high stability. Thus, the baselines we obtained are very flat. Therefore, only baselines of order zero or one were subtracted from the spectra, and the data were smoothed to a resolution of $\sim 10\,\mathrm{km\,s^{-1}}$.

From continuum cross scans on nearby sources, made every $\sim$ 3 hours, we estimate the pointing accuracy to be of order $5''$ or better. To check the calibration of the telescope, we usually observed line emission from strong Galactic sources like W3(OH) in each period to achieve internal consistency. We expect the calibration to be correct on a level of $\sim \pm 15\%$.

3. Results

3.1. Formaldehyde

The parameters of Gaussian fits to the detected lines are given in Table 2. Spectra are displayed in Fig. 1. Since not all lineshapes are exactly Gaussian, we have also determined the integrated line intensities by adding the channels with emission, calculating the errors from the rms noise per channel. The results are identical, with the errors of the Gaussian typically being slightly larger than the errors obtained using the rms noise.

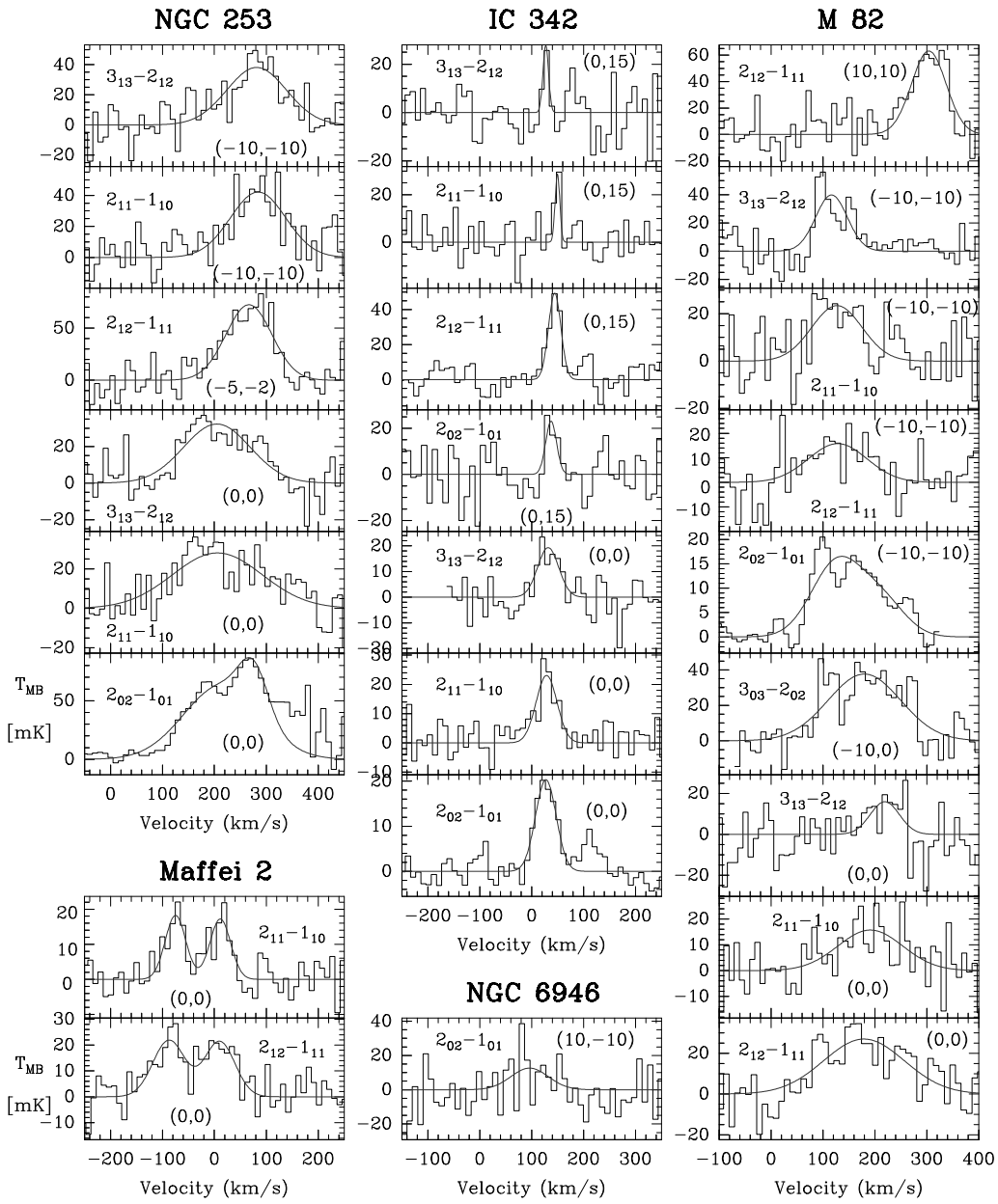

Fig. 1. H_2CO spectra for those positions and transitions where we detected, at least tentatively, a line. All spectra have been smoothed to a resolution of 10 km s^{-1}. The central positions (1950.0) and distances of the galaxies are: NGC 253: $\alpha = 00^h45^m06.0^s$, $\delta = -25°33'36''$, 2.5 Mpc, Maffei 2: $\alpha = 02^h38^m08.5^s$, $\delta = 59°23'24''$, 5 Mpc, IC 342: $\alpha = 03^h41^m57.5^s$, $\delta = 67°56'25''$, 1.8 Mpc, M 82: $\alpha = 09^h51^m43.0^s$, $\delta = 69°55'00''$, 3.3 Mpc, NGC 6946: $\alpha = 20^h33^m48.0^{sec}$, $\delta = 59°59'00'$, 11 Mpc.

We detected mm wavelength H_2CO transitions toward all galaxies that were observed, although the detection of the $2_{02} - 1_{01}$ line in NGC 6946 is tentative.

Toward NGC 253, four of the five transitions observed could be detected; in M 82, all five lines were found. The three positions observed in M 82 are detected in the $2_{12} - 1_{11}$ line, while the $2_{11} - 1_{10}$ line is not seen toward the (10″,10″) offset. Toward this position, the $J = 2 - 1$ twin lines thus have different intensities.

In IC 342, four out of six transitions were detected. It is interesting to note that the $3_{13} - 2_{12}$ transition was detected both toward the central and (tentatively) toward an offset position, while its twin transition, the $3_{12} - 2_{11}$ line, only observed toward the offset position, was not detected at an rms level of $\sim$12 mK. As in M 82, the intensities of the $J = 2 - 1$ twin lines differ. Toward the center, the $2_{11} - 1_{10}$ line is considerably stronger than its counterpart, the $2_{12} - 1_{11}$ transition, which is not detected.

Table 2. Parameters of H_2CO lines observed toward nearby spiral galaxies. The offsets from the central position are given in arcseconds. Errors (1σ) are given in parenthesis.

Source	Trans.	$\int T_{\rm MB} dv$	$v_{\rm LSR}$	$\Delta v_{1/2}$	$T_{\rm MB}$
		K km s^{-1}	km s^{-1}		mK
NGC253					
(0,0)	$2_{02}-1_{01}$ [a),b)]	~ 10	*210*	*170*	~ 45
	$3_{03}-2_{02}$	≤ 2.8 [c)]	–	–	≤ 17 [d)]
	$2_{11}-1_{10}$	6.1(0.7)	206(7)	204(25)	28(10)
	$3_{13}-2_{12}$	5.2(0.7)	205(10)	151(20)	32(11)
(–5,–2)	$2_{12}-1_{11}$	8.0(0.9)	267(6)	104(13)	72(13)
(–10,–10)	$2_{11}-1_{10}$	5.6(0.8)	284(7)	126(23)	42(11)
	$3_{13}-2_{12}$	5.5(0.7)	281(8)	136(26)	38(11)
Maffei2					
(0,0)	$3_{03}-2_{02}$	≤ 4.9	–	–	$\leq$33
	$2_{12}-1_{11}$	1.7(0.4)	–87(6)	74(18)	22(6)
		1.6(0.3)	10(6)	69(17)	21(6)
	$2_{11}-1_{10}$	0.9(0.2)	–75(4)	47(15)	19(4)
		0.9(0.2)	12(5)	45(11)	18(4)
	$3_{13}-2_{12}$	≤ 1.8	–	–	$\leq$12
	$3_{12}-2_{11}$	≤ 1.6	–	–	$\leq$11
IC342					
(0,0)	$2_{02}-1_{01}$ [b)]	1.0(0.1)	27(2)	47(5)	20(3)
	$2_{12}-1_{11}$	≤ 0.9	–	–	$\leq$16
	$2_{11}-1_{10}$	1.2(0.2)	29(4)	47(11)	23(5)
	$3_{13}-2_{12}$	1.0(0.2)	32(6)	48(12)	19(7)
(0,5)	$3_{03}-2_{02}$	≤ 3.3	–	–	$\leq$40
(0,15)	$2_{02}-1_{01}$	0.6(0.2)	38(5)	25(5)	23(10)
	$2_{12}-1_{11}$	1.5(0.2)	44(2)	28(5)	49(7)
	$2_{11}-1_{10}$	0.3(0.2) [e)]	50(2)	11(3)	29(7)
	$3_{13}-2_{12}$	0.4(0.2) [e)]	27(3)	13(6)	28(9)
	$3_{12}-2_{11}$	≤ 0.9	–	–	$\leq$12
M82					
(0,0)	$2_{02}-1_{01}$ [a)]	≤ 3.0	–	–	$\leq$30
	$2_{12}-1_{11}$	5.3(0.9)	179(17)	183(37)	27(9)
	$2_{11}-1_{10}$	2.5(0.6)	191(18)	147(44)	16(9)
	$3_{13}-2_{12}$	1.3(0.4) [e)]	219(16)	66(25)	16(10)
(–10,0)	$3_{03}-2_{02}$ [f)]	6.6(0.5)	180(6)	165(12)	38(8)
(–10,–10)	$2_{02}-1_{01}$ [a),b)]	~ 1.8	*120*	*110*	~ 15
	$2_{12}-1_{11}$	2.2(0.5)	128(18)	133(31)	16(10)
	$2_{11}-1_{10}$	2.9(0.6)	127(10)	114(34)	23(11)
	$3_{13}-2_{12}$	3.0(0.5)	117(8)	71(14)	40(11)
(10,10)	$2_{12}-1_{11}$	5.3(0.6)	304(5)	79(10)	63(13)
	$2_{11}-1_{10}$	≤ 0.8	–	–	$\leq$10
NGC6946					
(10,-10)	$2_{02}-1_{01}$	1.1(0.5) [e)]	96(18)	85(22)	13(11)

a) In NGC 253 and M 82, the $2_{0,2}-1_{0,1}$-line is blended with the 16–15 transition of HC_3N, offset by 42 MHz (86.5 km s^{-1}). An approximate fit for NGC 253 was obtained by fixing the central velocity and width of the HC_3N line to the values known from the 15–14 and 17–16 HC_3N transitions (Mauersberger et al. 1990). For M 82, the H_2CO line parameters were fixed to the mean value derived from unblended H_2CO lines in the same position, assuming the nominal offset for HC_3N. Both estimates are indicated by italics.

b) Data from Mauersberger et al. 1995

c) Limits for the integrated intensity are 3σ limits, based on the rms per channel extrapolated to a linewidth fixed to the value determined from detected H_2CO transitions toward the same position.

d) All limits and errors to $T_{\rm MB}$ are rms in a 10 km s^{-1} wide channel

e) tentative

f) Data from Baan et al. 1990

Toward a northern offset position however, the $2_{12}-1_{11}$ line is stronger than the (tentatively detected) $2_{11}-1_{10}$ line.

Toward Maffei 2, two out of four lines were found. The profiles show a double peaked structure. This double feature is also visible in the HNC(1–0) transition (Hüttemeister et al. 1995), but is not seen in other molecular species.

3.2. Methanol

The results of Gaussian fits for all observations of single positions are given in Table 3; spectra are displayed in Fig. 2. We also obtained a map of NGC 253 in the $J_{\rm k}=3_{\rm k}-2_{\rm k}$ transitions at 145 GHz with a 10″ spacing (Fig. 3).

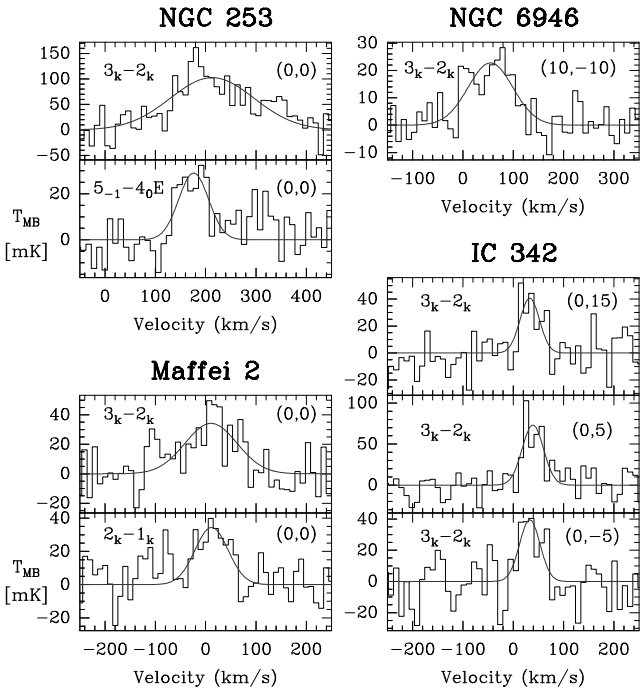

Fig. 2. CH_3OH transitions detected toward NGC 253, Maffei 2, IC 342 and NGC 6964.

As is the case for the $J=2_{\rm k}-1_{\rm k}$ transitions at 96 GHz, the $J=3_{\rm k}-2_{\rm k}$ 'line' is actually a blend of several individual transitions (see Table 1) with frequencies ranging from 145.09375 GHz to 145.13346 GHz, corresponding to a velocity shift of 82 km s^{-1}. We adopted a rest frequency of 145103.23,GHz, corresponding to the $3_0-2_0A^+$ transition. The $3_{\rm k}-2_{\rm k}$ transitions were detected with relative ease in all sources we observed, with the notable exception of M 82. In Maffei 2, the $2_{\rm k}-1_{\rm k}$ line was also easily detected. The $5_{-1}-4_0E$ transition in NGC 253 is clearly detected.

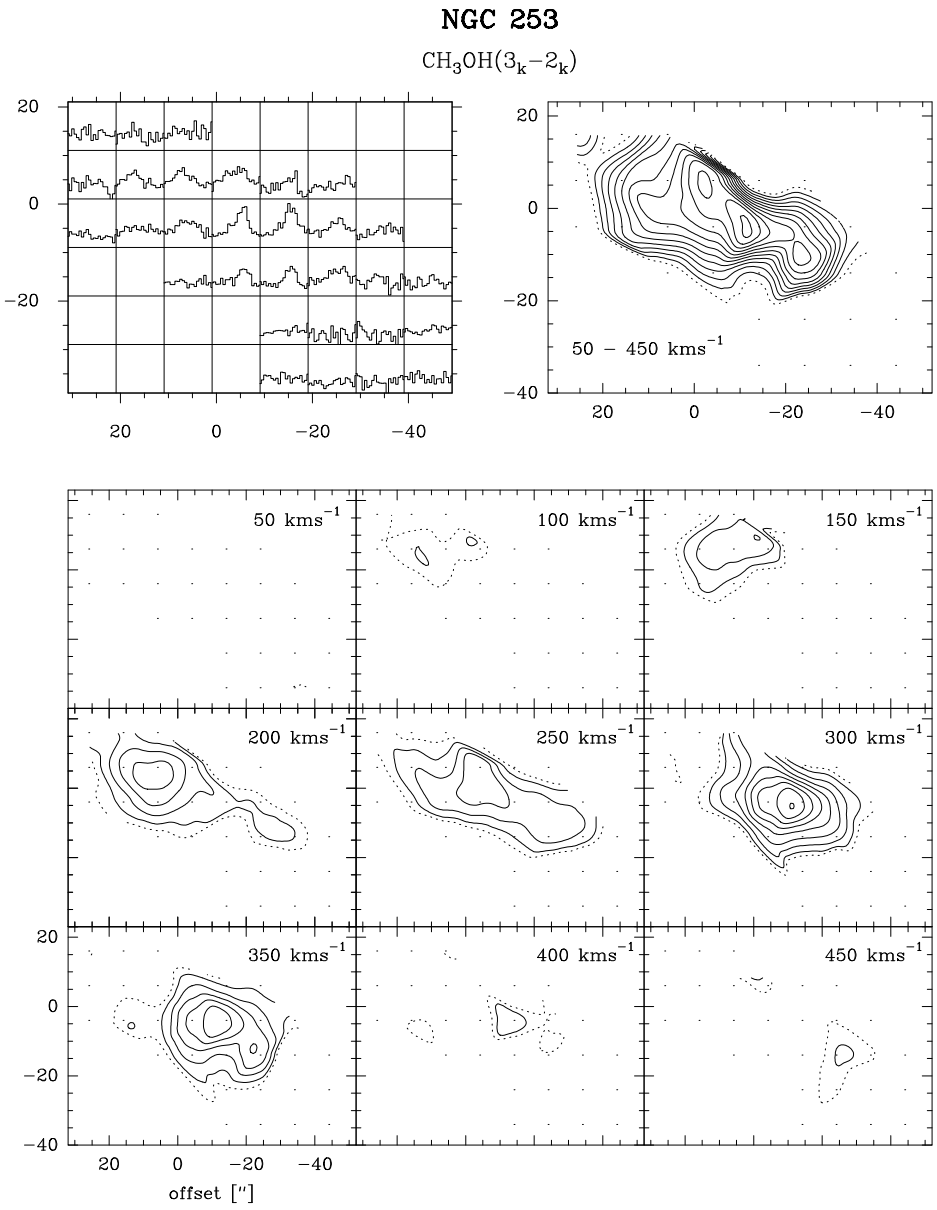

Fig. 3. Map of CH_3OH ($3_k - 2_k$) toward NGC 253. The upper left panel shows the spectra with a v_{LSR} range of 50–450 kms and T_{MB} ranging from –70 to 200 mK. The total integrated intensity map is given in the upper left panel; solid contours start at $5.25\,K\,km\,s^{-1}$ (3σ) in steps of $1.75\,K\,km\,s^{-1}$ (1σ). The dashed contour denotes the 2σ level at $3.5\,K\,km\,s^{-1}$. In the lower panel, we present channel maps of $50\,km\,s^{-1}$ width. The first solid contour is at $1.8\,K\,km\,s^{-1}$ (3σ), the steps are $0.9\,K\,km\,s^{-1}$; the dashed contour is $1.2\,K\,km\,s^{-1}$ (2σ).

4. Discussion

4.1. Physical conditions

4.1.1. H_2CO

Formaldehyde is a slightly asymmetric top molecule that exists in ortho- ($K_a = 1, 3, 5\ldots$) and para- ($K_a = 0, 2, 4\ldots$) forms that are not connected by allowed transitions. Thus, they can be considered independent molecular species. The asymmetry splits each rotational level in the $K_a > 0$-ladders into a so-called K-doublet (see, e. g., Henkel (1980) for a level diagram and more details).

Since relative populations of different K_a ladders are determined by collisions, line intensity ratios of transitions from different K_a ladders of a given species are excellent tracers of the gas kinetic temperature (Mangum & Wootten 1993). The level populations *within* a K_a ladder are

Table 3. Parameters of CH_3OH lines observed toward nearby spiral galaxies. The offsets from the central position are given in arcseconds.

Source	Trans.	$\int T_{\rm MB} dv$	$v_{\rm LSR}$	$\Delta v_{1/2}$	$T_{\rm MB}$
		K km s^{-1}	km s^{-1}		mK
NGC253					
(0,0)	$5_{-1} - 4_0 E$	2.2(0.4)	176(6)	70(12)	29(9)
	$2_{\rm k} - 1_{\rm k}^{\rm a)}$	3.8(0.6)	190(5)	70(12)	51(15)
		14.9(0.7)	309(2)	104(6)	136(15)
	$3_1 - 2_1 A^+$	$\leq 2.7^{\rm b)}$	–	–	≤ 20(18)
	$3_{\rm k} - 2_{\rm k}$	21.4(1.8)	213(8)	196(21)	102(25)
	$8_{-1} - 7_0 E$	≤ 2.0	–	–	≤ 15
	$3_{-2} - 4_{-1} E$	≤ 5.4	–	–	$\leq$19
Maffei2					
(0,0)	$5_{-1} - 4_0 E$	≤ 1.6	–	–	$\leq$12
	$2_{\rm k} - 1_{\rm k}$	2.8(0.7)	12(10)	77(33)	34(12)
	$3_1 - 2_1 A^+$	≤ 0.6	–	–	$\leq$6
	$3_{\rm k} - 2_{\rm k}$	4.4(0.7)	10(10)	122(26)	34(11)
	$8_0 - 7_1 E$	≤ 3.9	–	–	$\leq$39
	$8_{-1} - 7_0 E$	≤ 2.7	–	–	$\leq$27
IC342					
(0,0)	$5_{-1} - 4_0 E$	≤ 1.1	–	–	$\leq$16
	$3_{-2} - 4_{-1} E$	≤ 2.1	–	–	$\leq$31
(0,–5)	$3_{\rm k} - 2_{\rm k}$	2.0(0.4)	33(6)	48(9)	40(13)
(0,5)	$2_{\rm k} - 1_{\rm k}^{\rm a)}$	4.6(0.3)	46(2)	63(3)	68(15)
	$3_{\rm k} - 2_{\rm k}$	3.9(0.6)	39(3)	50(9)	73(14)
(0,15)	$5_{-1} - 4_0 E$	≤ 0.7	–	–	$\leq$11
	$3_{\rm k} - 2_{\rm k}$	2.0(0.5)	33(6)	46(12)	41(13)
	$8_0 - 7_1 E$	≤ 2.6	–	–	$\leq$39
	$3_{-2} - 4_{-1} E$	≤ 1.5	–	–	$\leq$22
M82					
(0,0)	$5_{-1} - 4_0 E$	≤ 1.1	–	–	$\leq$10
	$3_{\rm k} - 2_{\rm k}$	≤ 2.3	–	–	$\leq$15
	$8_0 - 7_1 E$	≤ 2.4	–	–	$\leq$18
	$3_{-2} - 4_{-1} E$	≤ 1.6	–	–	$\leq$11
(–10,0)	$2_{\rm k} - 1_{\rm k}^{\rm a)}$	≤ 3.3	–	–	$\leq$34
(–10,–10)	$5_{-1} - 4_0 E$	≤ 1.1	–	–	$\leq$10
	$3_{\rm k} - 2_{\rm k}$	≤ 1.8	–	–	$\leq$11
	$8_0 - 7_1 E$	≤ 1.2	–	–	$\leq$11
	$3_{-2} - 4_{-1} E$	≤ 1.8	–	–	$\leq$16
(10,10)	$3_{\rm k} - 2_{\rm k}$	≤ 1.7	–	–	$\leq$15
	$8_0 - 7_1 E$	≤ 2.5	–	–	$\leq$25
NGC 6946					
(4,0)	$2_{\rm k} - 1_{\rm k}^{\rm a)}$	1.7(?)	55(?)	100(?)	17(?)
(10,–10)	$5_{-1} - 4_0 E$	≤ 0.7	–	–	≤ 6
	$3_1 - 2_1 A^+$	≤ 0.8	–	–	$\leq$7
	$3_{\rm k} - 2_{\rm k}$	2.5(0.3)	54(7)	105(15)	23(5)
	$8_0 - 7_1 E$	≤ 1.5	–	–	$\leq$13
	$3_{-2} - 4_{-1} E$	≤ 1.4	–	–	$\leq$12

a) Results taken from Henkel et al. 1987.
b) Limits to the integrated intensity and $T_{\rm MB}$ were derived as for H_2CO (Table 2)

determined by an equilibrium between collisional excitation and spontaneous and collisional deexcitation, making the relative level populations within a $K_{\rm a}$ ladder sensitive to the H_2 density and, to a lesser degree, to kinetic temperatures.

We have carried out large velocity gradient (LVG) statistical equilibrium computations of the population of the $K_{\rm a} = 1$ ladder of ortho formaldehyde (o-H_2CO), for which we have the most complete data. The model is described in detail in Henkel et al. (1980). We included 16 levels of that rotational ladder fixing the kinetic temperatures to a value of 80 K. Setting $T_{\rm kin}$ to 50 K changes the line intensity ratios only by a few percent. As a result of these calculations, line ratios for the 140, 150 and 211 GHz transitions of o-H_2CO are related to the H_2 density and the H_2CO column density per unit linewidth (see Fig. 4).

It is evident from Fig. 4 that the 1.3 mm and 2 mm lines have similar intensities if densities exceed 10^5 cm^{-3} (this also holds for para formaldehyde). In order to derive column densities of o-H_2CO from the integrated intensities of one or several lines, an assumption must be made about the H_2 density and, to a lesser degree, the kinetic temperature, both of which determine the rotational temperature, or more generally, the partition function. An integrated intensity of 1 K kms^{-1} of the 140 GHz line corresponds e.g. to $N({\rm o-H_2CO}) \sim 5\,10^{13}\,{\rm cm^{-2}}$ if one assumes a low H_2 density of 10^4 cm^{-3}; if, however, $n(H_2) = 10^5 - 10^7$ cm^{-3} is assumed, then the o-H_2CO column densities for the same line intensity are an order of magnitude lower. In Table 4, we estimate $N({\rm o-H_2CO})$ from the intensities of the 140 GHz lines, and the densities from the measured line intensity ratios. The most reliable densities from mm-wave line intensity ratios are estimated for regions where $n(H_2) > 10^5$ cm^{-3}. For lower densities, mm-wave lines of H_2CO become optically thick if $N({\rm o-H_2CO})/\Delta v \gtrsim 10^{12.5}\,{\rm cm^{-2}/km\,s^{-1}}$. In this case, the line intensity ratios not only depend on $n(H_2)$, but also strongly on $N({\rm o-H_2CO})/\Delta v$. Upper limits on $n(H_2)$ estimated in Table 4 are based on the optically thin limit.

In order to determine relative abundances, the H_2 column density has to be known. In Table 4, we use values deduced from CO measurements, and the standard conversion formula of Strong et al. (1988), i.e. $\eta N(H_2)/I({\rm CO}) = 2.3 10^{20}\,{\rm cm^{-2}\,(K\,km\,s^{-1})^{-1}}$. However, there is growing evidence that this conventional conversion factor cannot be applied to Galactic bulge regions (see Dahmen et al. 1996a,b for our Galactic center, Mauersberger et al. 1996a,b for NGC 253 and NGC 4945, Shier et al. 1994 for IR-luminous galaxies). The correction factor η might be as large as 10, and is likely to be different for different galaxies. It will, however, always decrease H_2 column densities and increase the relative abundance of the molecule.

NGC 253. Toward this galaxy, we have the largest data base. In order to compare line intensities which have been obtained at different wavelengths one has to take into ac-

count the different beam sizes and the spatial structure of the source. Since we did not map the distribution of H_2CO toward any of our sources, we assume that the distribution of this molecule toward NGC 253 is similar to that of the $J = 2 - 1$ line of ^{12}CO, which has been mapped with $12''$ resolution and convolved to different resolutions by Mauersberger et al. (1996a). From an interpolation of the data toward the central position of NGC 253 in their Table 1, intensities in a $16''$ beam are a factor 0.85 weaker than data at $12''$ resolution. In the following analysis we assume the same correction factor for the 2 mm data of M 82 and IC 342 where the size of the molecular emission is similar to that of NGC 253.

We can use the intensity ratios of lines within the $K_a = 1$ ladder of ortho formaldehyde to estimate the H_2 density of the H_2CO emitting gas. In practice, a difficulty in assessing the line ratios arises if the line shapes and/or the velocity coverage differs. One might then incorrectly compare different gas components. The $3_{13} - 2_{12}$ (211 GHz) and the $2_{12} - 1_{11}$ (140 GHz) lines were observed toward slightly different positions, adding to the uncertainty. If only the clear overlap region in the spectra is considered, a line intensity ratio of $0.42(\pm 0.07)$ results. From Fig. 4 such a low ratio is compatible with $n(H_2) \sim 10^4\,cm^{-3}$, and even lower densities if H_2CO lines are saturated. We conclude that $n(H_2) < 10^5\,cm^{-3}$ for the bulk of the H_2CO emitting gas. From our limit to the $3_{03} - 2_{02}$ line and the detection of the $2_{02} - 1_{01}$ line of para H_2CO, the corresponding ratio is < 0.2 which is compatible with $n(H_2) \leq 10^4\,cm^{-3}$.

The ratio of the $2_{11} - 1_{10}$ (ortho, 150 GHz) and the $2_{02} - 1_{01}$ (para, 146 GHz) transitions depends on the ortho/para (o/p) ratio. For the high temperature limit of the o/p ratio of 3, one would expect a line intensity ratio of ~ 1.4 (for $T_{kin} = 80\,K$) and $n(H_2) = 10^4\,cm^{-3}$. The value we actually observe is 0.6, or even lower, if one argues that not the entire velocity range for the wide $2_{11} - 1_{10}$ line should be considered for the ratio. We therefore suggest that the o/p ratio of H_2CO actually has a value close to 1, which is lower than the value derived by Aalto et al. (1997) for the 1 mm transitions. Since the o/p ratio bears important information on the formation of molecular gas, and our result, involving a blended line, is uncertain, further observations are very desirable.

M 82. We have measured ortho-H_2CO lines toward two positions in M 82, namely toward the nucleus and toward the so called SW molecular hotspot at an offset of $(\Delta\alpha, \Delta\delta) = (-10'', -10'')$ (Mauersberger & Henkel 1991). The ratio (for the same beam size) of the $3_{13} - 2_{12}$ (211 GHz) and the $2_{12} - 1_{11}$ (140 GHz) lines is ≤ 0.2 toward the nucleus, regarding the tentatively detected $3_{13} - 2_{12}$ as contributing an upper limit only. Toward the SW hotspot, however, it is as high as $1.2(\pm 0.4)$, or even ~ 1.5, if we restrict the intensity from the $2_{12} - 1_{11}$ line to the width of the slightly narrower $3_{13} - 2_{12}$ transition.

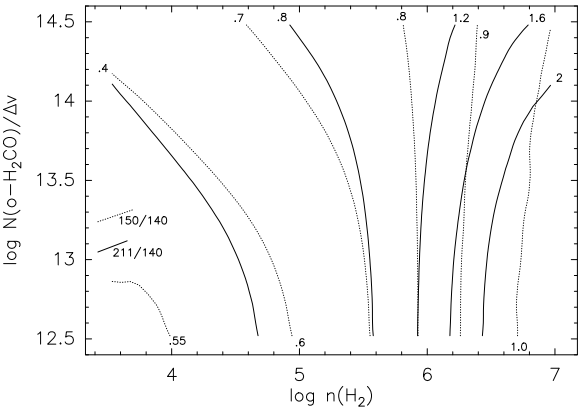

Fig. 4. Predicted line intensity ratios of ortho-formaldehyde lines as a function of $n(H_2)$ (in cm^{-3}) and $N(\text{ortho-}H_2CO)/\Delta v$ (in $cm^{-2}/(km\,s^{-1})$. Solid contours: $T_B(211\,GHz)/T_B140\,GHz)$, thin contours: $T_B(150\,GHz)/T_B(140\,GHz)$. The assumed T_{kin} is 80 K.

Thus, toward the nucleus, $n(H_2) < 10^4\,cm^{-3}$; while densities are as high as $n(H_2) \sim 10^6\,cm^{-3}$ toward the SW hotspot. This estimate is relatively robust to whether or not the H_2CO lines are saturated.

Such density variations were already predicted from an analysis of centimeter wave transitions of ortho formaldehyde observed with lower angular resolution by Baan et al. (1990). While the 6 cm line shows a broad absorption (Graham et al. 1978) over the entire velocity range, the 2 cm line is seen in emission over a velocity range that hints toward an origin which is confined toward the southwestern part of the nuclear region. The 2 cm H_2CO line is usually observed in absorption, even against the 2.7 K cosmic background. 2 cm emission requires H_2 densities exceeding $10^{5.5}\,cm^{-3}$. This is in very good agreement with our results from millimetric lines toward the SW hotspot. Also the central concentration of N_2H^+, a molecular ion that is destroyed in a high density medium, indicates that the gas toward the central region has a much lower density than toward the SW hotspot (Mauersberger & Henkel 1991).

From the observed line intensity ratio of the $2_{12} - 1_{11}$ and $2_{02} - 2_{01}$ lines of ~ 1.2, the o/p ratio toward the SW hotspot is (assuming $n(H_2) = 10^6\,cm^{-3}$) ~ 2, i.e. close to the high temperature limit. Note, however, that, as for NGC 253, this result may be affected by the uncertainty of the fit to the blended $2_{02} - 2_{01}$ transition.

IC 342. This nearby (~ 2 Mpc; McCall 1989, Karachentsev & Tikhonov 1993) and nearly face-on spiral galaxy is very similar to the Milky Way galaxy with respect to the IR luminosity and the gas mass in its central region.

We have observed formaldehyde toward the nucleus $(0'', 0'')$, where the velocity coverage and the line shapes of all transition are in excellent agreement, and toward one offset position, $(0'', 15'')$, where the (tentative) $3_{13} - 2_{12}$

transition seems to appear at a different velocity. The beam toward the $(0'', 0'')$ position also contains the molecular clump B (Downes et al. 1992), which is associated with free-free emission equivalent to 300 O5 stars or 30 times more than the emission from the Galactic center star forming region Sgr B2.

$3_{13} - 2_{12}/2_{11} - 1_{10}$ (211 GHz/150 GHz) line ratios indicate high densities of $10^{6.2}$cm^{-3} toward the $(0'', 0'')$ position. The limit to the $2_{11} - 1_{10}/2_{12} - 1_{11}$ (140 GHz/150 GHz) line ratio toward the nucleus of ≥ 1 is also suggesting high densities, while the limit toward the $(0'', 15'')$ offset (≤ 0.4, considering the tentative detection to be an upper limit, and regarding a common velocity interval for both lines), indicates a far lower density of $< 10^4$ cm^{-3}. As in M 82, our two beams pick up contributions from two molecular phases, namely from a moderately dense interclump gas and from the clumps themselves. The presence of several molecular gas components has also been inferred by Downes et al. (1992) from the comparison of single dish and interferometric observations in CO.

Maffei 2. The ratios of the 150 and 140 GHz line, which agree very well in velocity coverage and line shape, indicate typical densities of the order of 10^4 cm^{-3}.

4.1.2. CH_3OH

Methanol is an asymmetric top molecule capable of hindered internal rotation. Transitions from A-type (internal rotation) to E-type (no internal rotation) levels are strictly forbidden; the two types behave as separate molecular species in the ISM. In addition, *a* and *b*-type transitions have to be distinguished according the component of the dipole moment that is is parallel to the axis of rotation. All transitions contributing to the $3_k - 2_k$ and $2_k - 1_k$ lines are *a*-type ($\Delta k = 0; \mu_a = 0.896$ Debye), while the $5_{-1} - 4_0$ transition is *b*-type ($\Delta k = 1; \mu_b = 1.412$ Debye) (Lees et al. 1973, Sastry et al. 1981; for a detailed discussion of the CH_3OH molecule, see e. g. Menten 1987).

An analysis of the $3_k - 2_k$ group of transitions is difficult since the lines are blended. We have, however, carried out LVG calculations analogous to those for H_2CO, using a program provided by C.M. Walmsley (see, e.g. Walmsley et al. 1988, Bachiller et al. 1995). We have modelled the intensity ratios of the sum of all transitions contributing to the $3_k - 2_k$ group to the sum of the $2_k - 1_k$ transitions and the ratio of the $3_k - 2_k$ group to the $5_{-1} - 4_0 E$ line as a function of H_2 density and CH_3OH column density per unit linewidth (Fig. 5), for a kinetic temperature of 80 K. Clearly, for $N(CH_3OH)/\Delta v \lesssim 10^{14}\,\mathrm{cm^{-2}/km\,s^{-1}}$, the line ratios are independent of column density. Thus, the CH_3OH lines are very likely to be optically thin in all our sources. We have used the H_2 densities determined from Fig. 5 and the integrated intensities of the $3_k - 2_k$ group of transitions to determine the CH_3OH column densities given in Table 4.

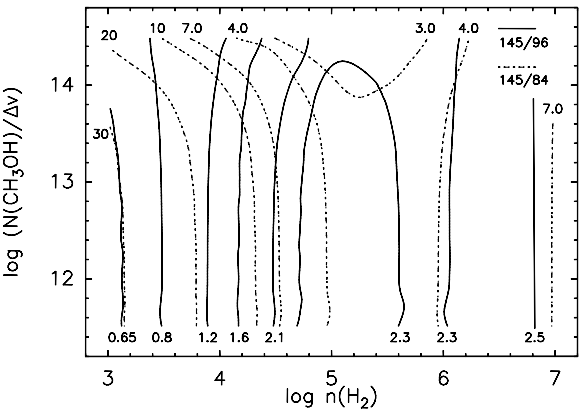

Fig. 5. Predicted intensity ratios of methanol lines for a raster of values for $n(H_2)$ (in cm^{-3}) and $N(CH_3OH))/\Delta v$ (in cm^{-2}/(km s^{-1}). Solid contours: $T_B(145\,\mathrm{GHz})/T_B(96\,\mathrm{GHz})$, dashed contours: $T_B(145\,\mathrm{GHz})/T_B(84\,\mathrm{GHz})$. The assumed T_{kin} is 80 K.

Table 4. Beam averaged H_2CO and CH_3OH column densities and relative abundances.

Source	ηN	N	N	$\frac{[H_2CO]}{[H_2]\eta}$	$\frac{[CH_3OH]}{[H_2]\eta}$
	H_2 [a]	H_2CO	CH_3OH		
	10^{22}	10^{13} cm^{-2}	10^{13}	10^{-9}	10^{-9}
NGC 253					
(0,0)	37	40 [b]	50 [b]	1.1	1.4
M 82					
(0,0)	16	~ 25 [c]	≤ 2 [e]	1.6	≤ 0.1
(–10,–10)		0.9 [d]	$\leq$ 1–2 [e]		
IC 342					
(0,0)	4.9	0.2 [d]		0.04	
(0,5)	4.9		11 [f]		2.2
(0,–5)			6 [f]		
(0,15)		> 8 [c]	6 [f]		
Maffei 2	1.4	15 [b]	4 [b]	11	2.9
NGC 6946	2.3		3 [b]		1.3

a) based on I(CO) (see Hüttemeister et al. 1995 and references therein) and a "conventional" conversion factor.
b) assumed $n(H_2)$: $\sim 10^4$ cm^{-3}
c) assumed $n(H_2)$: $< 10^4$ cm^{-3}
d) assumed $n(H_2)$: $\sim 10^6$ cm^{-3}
e) from Eq. 1; with T_{rot} =10 K
f) assumed $n(H_2)$: $\gtrsim 10^3$ cm^{-3}

NGC 253. The map we obtained in the $3_k - 2_k$ transition toward NGC 253 (Fig. 3) shows the same general shape as maps in other high density tracing molecules like HNC (Hüttemeister et al. 1995) and CS (Mauersberger & Henkel 1989). The emission extends from the north-east to the south-west, with a (not deconvolved) full source size of $\sim 55'' \times 25''$, which is similar to the extent of intense ^{12}CO(2–1) emission (Mauersberger et al. 1996a).

Therefore, it seems reasonable to correct the $3_k - 2_k/2_k - 1_k$ and the $3_k - 2_k/5_{-1} - 4_0 E$ line ratios for the different beamsizes in the same way as for H_2CO (Section 4.1.1), based on the Mauersberger et al. (1996a) data. The line intensities of the 3 mm lines then have to be multiplied by ~ 1.4 to make them directly comparable to the 2 mm lines. The linewidths of the two groups of transitions agree well. The resulting $3_k - 2_k/2_k - 1_k$ ratio (0.8±0.15) implies a H_2 density of $\sim 10^{3.5}\,\mathrm{cm}^{-3}$. The $5_{-1} - 4_0$ line is much narrower than the $3_k - 2_k$ group. Since we are comparing a group of transitions spaced by $> 80\,\mathrm{km\,s}^{-1}$ to an unblended line, this is to be expected. However, it might not account for the entire difference. The ratio of the integrated intensities (6.8±2.4) thus is an upper limit, yielding a lower limit to the density of $10^{4.5}\,\mathrm{cm}^{-3}$. If we consider only the velocity interval for the $3_k - 2_k$ group where $5_{-1} - 4_0$ emission is present, this lower limit to the intensity ratio of 3.1±0.7 corresponds to a an upper limit to the H_2 density of $\geq 10^5\,\mathrm{cm}^{-3}$(see Fig. 5). In any case, the values from the $3_k - 2_k/2_k - 1_k$ and the $3_k - 2_k/5_{-1} - 4_0$ line ratios embrace the H_2 density estimated from H_2CO. The critical density of the $5_{-1} - 4_0 E$ transition is smaller than the mean of the $3_k - 2_k$ group by a factor of ~ 5, while the difference is much less pronounced between the $3_k - 2_k$ and the $2_k - 1_k$ groups. This might explain the difference in the density estimates resulting from the two line intensity ratios.

At an H_2 density close to $10^4\,\mathrm{cm}^{-3}$, both the $2_k - 1_k$ and the $3_k - 2_k$ groups of lines are subthermally excited ($T_{ex} < T_{kin}$), with excitation temperatures for the individual transitions ranging from 10 K to 20 K. We thus obtain a value for $N(CH_3OH)$ which is lower by a factor of ~ 6 than what is determined under the assumption that the density is sufficiently high to thermalize the CH_3OH emission (Henkel et al. 1987).

M 82. The clear non-detection of any methanol line in M 82 is one of our most striking results. Henkel et al. (1987) searched for the $2_k - 1_k$ transition in this galaxy and established an upper limit of 30 mK rms T_{MB} for this line. We obtained upper limits of 10–15 mK rms for the $3_k - 2_k$ transition toward the central position and the north-eastern and south-western peak positions of the molecular ring.

Since no line ratios could be determined, we have used the LTE approximation for optically thin lines to estimate the total CH_3OH column density:

$$N(CH_3OH) = 1.28\,T_{rot}^{1.5}\,e^{E_l/kT_{rot}}\,\frac{1.67\,10^{14}}{\nu\mu^2 S}\int T_{MB}\,dv \qquad (1)$$

(E_l: Energy of lower level, ν: line frequency in GHz, μ: dipole moment in Debye, S: linestrength; Menten et al. 1988).

Using Eq. 1, we have fitted all components of the $3_k - 2_k$ group to the limit to the integrated intensity. For subthermally excited lines ($T_{rot} = 10$ K), we find column densities ranging from smaller than $1\,10^{13}\,\mathrm{cm}^{-2}$ (SW hotspot) to less than $2\,10^{13}\,\mathrm{cm}^{-2}$ (center and NE hotspot), corresponding to an abundance of $[CH_3OH]/\eta[H_2] \leq 1.2 10^{-10}$ (see Table 4). If we assume that the H_2 densities are the same as the ones found for H_2CO and apply our LVG model, the only change is a slight increase in the limit for $N(CH_3OH)$ to $2\,10^{13}\,\mathrm{cm}^{-2}$ in the dense SW hotspot (see Table 4).

IC 342. Within the $3_k - 2_k$ blend, two groups of lines are separated by $\sim 45\,\mathrm{km\,s}^{-1}$. The group of 5 lines at higher frequency has generally higher energies than the lower frequency group. Because the lines in IC 342 are narrow, these two groups are resolved, and the higher energy transitions are below the detection limit. Thus, LTE fits to the $3_k - 2_k$ group already greatly constrain the possible excitation conditions: T_{rot} has to be 10 K or lower. Since the kinetic temperature of the gas in IC 342 is likely to be at least 50 K (Ho et al. 1990), CH_3OH has to be very subthermally excited, with T_{ex} lower than for NGC 253.

The LVG calculations confirm this: For a (beam size corrected) $3_k - 2_k/2_k - 1_k$ intensity ratio of 0.6(±0.1), observed toward the (0″,5″) position, we find an H_2 density of only $\sim 10^3\,\mathrm{cm}^{-3}$ ($T_{kin} = 80$ K) to $\sim 10^{3.4}\,\mathrm{cm}^{-3}$ ($T_{kin} = 50$ K) and excitation temperatures of $\sim 5 - 10$ K. This implies that CH_3OH is sensitive to interclump gas of only low to moderate density.

The beam-averaged column density we derive is $1.1\,10^{14}\,\mathrm{cm}^{-2}$ for a position slightly north of the center of IC 342, and half that for offsets to the south and further to the north (assuming the same low density), corresponding to an abundance of $[CH_3OH]/\eta[H_2] \sim 2\,10^{-9}$ (Table 4). We note that the column densities given in Henkel et al. (1988), based on $T_{rot} = 50$ K and derived from the $2_k - 1_k$ line, are far too high. A recalculation using $T_{rot} = 8$ K and Eq. 1 (with $\sum S_i = 7$ and $E_l = 6$ K) yields a total column density that agrees to within 10% with our result for the $3_k - 2_k$ line, showing that the LTE and LVG approximations converge in this case. The limit given by the non-detection of the $5_{-1} - 4_0$ transition is also compatible with a total CH_3OH column density of $\sim 10^{14}\,\mathrm{cm}^{-2}$.

Maffei 2 and NGC 6946. The $3_k - 2_k/2_k - 1_k$ line ratios, corrected for beam size, imply H_2 densities of $\sim 10^4\,\mathrm{cm}^{-3}$.

It thus seems likely that the excitation of CH_3OH in both galaxies is similar to what is found in NGC 253.

4.2. Chemical variations

Molecular abundances. For most of the galaxies observed, the column densities of o-H_2CO and CH_3OH are comparable. This might also be the case for the M 82 SW hotspot, where we have only a limit for the CH_3OH column density. The notable exception is the nucleus of M 82 where the column density of CH_3OH is at least an order of magnitude lower than that of H_2CO. It is quite clear that this is not just mimicked by excitation effects. Such a discrepancy between M 82 and other starburst galaxies, especially NGC 253, has already been noticed before (e.g. Mauersberger & Henkel 1993).

Evaporation from grain surfaces is in many cases a crucial process to maintain a high gas phase abundance of complex molecular species. Models predict that these molecules, such as CH_3OH and also H_2CO, are chemically converted into simpler species on a timescale of order 10^5 years (Helmich 1996). Methanol evaporates at a temperature around 70 K (Turner 1989, Nakagawa 1990) and is known to be a tracer of hot, dense gas (Menten et al. 1988), since its abundance is observed to increase dramatically in the vicinity of young massive stars.

Formaldehyde, on the other hand, empirically shows far smaller abundance variations in Galactic interstellar clouds (Mangum and Wootten 1993) although it is 3–25 times more abundant in the Orion hot core than in other molecular clouds (Mangum et al. 1990). Contrary to CH_3OH, H_2CO is also abundant in cirrus clouds (Turner 1993) and cool, dense Galactic disk sources. It seems certain that processing on dust grains must play a role in the chemistry of H_2CO, but the replenishment process is unclear (Federman & Allen 1991, Turner 1993, Liszt & Lucas 1995).

Takano et al. (1995) notice that all molecules that are known to be depleted in M 82 (besides CH_3OH also SiO, HNCO, CH_3CN and SO) form preferentially under high temperature conditions. In the presence of a steep gravitational potential and a central bar, we expect shocks and turbulence to play a significant role in the heating of molecular clouds distant from the actual sites of star formation (e.g. Hüttemeister et al. 1993, Das & Jog 1995). This can explain the high temperatures toward the central molecular condensation of NGC 253, which is much more compact than that of M 82, a smaller, irregular galaxy. Tidal heating should therefore operate less efficiently in M 82 than in larger spirals like NGC 253, NGC 6946 or IC 342. Thus, one would expect the bulk of the gas in the center of NGC 253 to be warmer than that toward the center of M 82 (with the exception of those clouds which are heated directly by newly formed stars).

The abundance of CH_3OH in NGC 253 does not seem to be exceptionally high when compared to NGC 6946 or non-starburst nuclei like Maffei 2 and IC 342. But we tentatively find that the gas traced by CH_3OH in NGC 253 is at a similar density as the gas traced by H_2CO, while the gas traced by CH_3OH close to the nucleus of IC 342 is at a lower density. If temperature is indeed the key to the distribution of CH_3OH, we may conclude that the warm gas in IC 342 is less dense than in NGC 253. Since IC 342 is not a starburst galaxy, this agrees with the fact that warm gas in the center of our Galaxy is, in the absence of massive star formation, at lower densities than cooler gas (Hüttemeister et al. 1993), while the opposite is expected for active star forming regions. NGC 253 might be lacking the high temperature, low density interclump gas component picked up by CH_3OH in IC342; the bulk of the molecular material in NGC 253 is warm, at least moderately dense gas. In this scheme, M 82 has a cooler interclump component, seen in H_2CO and N_2H^+ (Mauersberger & Henkel 1991), but not in CH_3OH.

Extended methanol emission in NGC 253. While the general shape of the central molecular condensation seen in CH_3OH and other molecules is similar, in a detailed comparison differences are apparent. The maps of total integrated intensity in $^{12}CO(2–1)$, CS and HNC all show only one central peak. Only when the red- and blueshifted emission is displayed separately, two distinct peaks, separated by $10'' - 15''$, become visible, with the redshifted emission centered toward the south-west. The CH_3OH map (Fig. 3) shows these two peaks even for the total velocity range. The positions of the peaks agree to within better than $5''$ with the 'red' and 'blue' peaks seen in the other molecules. From the channel maps, the blueshifted emission is strongest at $200\,km\,s^{-1}$ and the red-shifted emission peaks at $300\,km\,s^{-1}$. In addition, there is a third peak, visible in the intensity and channel maps, at an offset of $\sim(-25'',-10'')$, at an even higher velocity of $350 - 450\,km\,s^{-1}$.

Only the interferometric $^{12}CO(1–0)$ map obtained by Canzian et al. (1988) with a $5'' \times 9''$ beam also shows two resolved peaks (at the same positions as the CH_3OH peaks) when the total velocity range is considered. Thus, the single dish CH_3OH data match the interferometric data not only more closely than the single dish ^{12}CO data, but also better than single dish maps of other high density tracers, namely CS and HNC. Since the interferometer misses extended emission, we can conclude that CH_3OH traces a more confined gas component than CS or HNC. Since the critical densities of $CH_3OH(3_k - 2_k)$, CS(2–1) and HNC(1–0) are roughly similar at $\sim 3 - 6\,10^5\,cm^{-3}$, the differences in spatial distribution seem to be caused by chemical fractionation rather than gas density. Since production of CH_3OH is favored in high temperatures, the differences in distribution may reflect differences in gas temperatures within the generally at least moderately dense gas in the bulge of NGC 253, with CH_3OH preferentially tracing the sites of ongoing massive star formation.

5. Conclusions

We have observed rotational transitions of the high gas density tracing molecules H_2CO and CH_3OH toward a sample of nearby gas rich external galaxies, namely NGC 253, Maffei 2, IC 342, M 82 and NGC 6946. Our main results are:

1. H_2CO was detected in all 5 galaxies searched (tentatively in NGC 6946).
2. In the prominent starburst galaxy NGC 253, the bulk of the gas emitting H_2CO lines is at densities of $\sim 10^4\,\mathrm{cm}^{-3}$. In both M 82 and IC 342, the H_2CO line ratios distinguish two different components of molecular gas. High densities dominate the SW molecular hotspot in M 82 and the central region of IC 342 ($n(H_2) \approx 10^6\,\mathrm{cm}^{-3}$), while lower densities ($< 10^4\,\mathrm{cm}^{-3}$) are prevalent toward the center of M 82 and the north of the nucleus of IC 342.
3. We detected CH_3OH lines in the same sample of galaxies, with the notable exception of M 82.
4. In all galaxies detected, methanol is subthermally excited. In NGC 253, Maffei 2 and NGC 6946, moderate gas densities of $\sim 10^4\,\mathrm{cm}^{-3}$ are likely. Toward a position north of the center of IC 342, the H_2 densities seem to be at $\sim 10^3\,\mathrm{cm}^{-3}$. This might indicate that warmer gas is at lower densities in the non-starburst nucleus of IC 342, where CH_3OH traces an entirely different gas component than H_2CO.
5. In M 82, no methanol could be detected down to an rms level of 10–15 mK, corresponding to an abundance at least an order of magnitude lower than in the other galaxies. This confirms large scale chemical differences in starburst centers. The likeliest cause of these are global differences in the temperature of the molecular material.
6. A map of NGC 253 in the 3_k-2_k line of methanol shows several peaks of emission and a greater amount of spatial structure than than single-dish maps of of other molecules, even high-density tracers. Thus, CH_3OH emission is associated with smaller scale clumps. This indicates chemical fractionation not only between different galaxies but also within the bulge of NGC 253, possibly reflecting the temperature structure of the gas.

Acknowledgements. R.M. was supported by a Heisenberg fellowship by the Deutsche Forschungsgemeinschaft. We thank K. Menten and C.M. Walmsley for help with the interpretation of the methanol data, S. Aalto-Bergman, P. Jewell, J. Mangum, and S. Radford for useful discussions, and the referee, L.-Å. Nyman, for helpful comments.

References

Aalto S., Bergman P., Black J.H., 1997, to be submitted to ApJ
Anderson T., De Lucia F.C., Herbst E., 1990, ApJS 72, 797
Baan W.A., Haschick A.D., 1995, ApJ 454, 745
Baan W.A.,Güsten R., Haschick A.D., 1986, ApJ 305, 830
Baan W.A., Henkel C., Schilke P., et al., 1990, ApJ 353, 132
Baan W.A., Goss W.M., 1992, ApJ 385, 188
Baan W.A., Haschick A.D., Uglesich R., 1993, ApJ 415, 140
Bachiller R., Liechti S., Walmsley C.M., Colomer F., 1995, A&A 197, 271
Canzian B., Mundy L.G., Scoville N.Z., 1988, ApJ 333, 157
Cohen R.J., Few R.W., Booth R.S., 1979, MNRAS 187, 35P
Dahmen G., Hüttemeister S., Wilson T.L., et al., 1996, in: ASP Conf. Ser. 102: The Galactic Center, ed.: R. Gredel, p. 54
Dahmen G., Hüttemeister S., Wilson T.L., Mauersberger R., 1997, to be submitted to A&A
Das M., Jog C.J., 1995, ApJ 451, 167
Downes D., Radford S.J.E., Guilloteau S., et al., 1992, A&A 262, 424
Ellingsen S.P., Whiteoak J.B., Norris R.P., et al., 1994, MNRAS 269, 1019
Gardner F.F., Whiteoak J.B., 1974, Nat 247, 526
Gardner F.F., Whiteoak J.B., 1976 MNRAS 175, 9P
Gardner F.F., Whiteoak J.B., 1979 MNRAS 189, 51P
Graham D.A., Emerson D.T., Weiler K.W., et al., 1978 A&A 70, L69
Güsten R., 1989, in: The center of the Galaxy, ed.: M. Morris, Kluwer Dordrecht, p.89
Federman S.R., Allen M., 1991, ApJ 375, 157
Helmich F.P., 1996, Ph.D. Thesis, Leiden University
Henkel C., 1980, Ph.D. Thesis, Bonn University
Henkel C., Walmsley C.M., Wilson T.L., 1980, A&A 82, 41
Henkel C., Jacq T., Mauersberger R., Harju J., 1987, A&A 188, L1
Henkel C., Whiteoak J.B., Nyman L.-Å., et al., 1990, A&A 230, L5
Henkel C., Mauersberger R., Wiklind T., et al., 1993, A&A 268, L17
Ho P.T.P., Martin R.L., Turner J.L., Jackson J.M., 1990, ApJ 355, L19
Hüttemeister S., Wilson T.L., Bania T.M., Martín-Pintado J., 1993, A&A 280, 255
Hüttemeister S., Henkel C., Mauersberger R., et al., 1995, A&A 295, 571
Johansson L.E.B., Olofsson H., Hjalmarson A., et al., 1994, A&A 291, 89
Karachentsev I.D., Tikhonov N.A., 1993, A&AS 100, 227
Lees R.M., Lovas F.J., Kirchhoff W.H., Johnson D.R., 1973, J. Phys. Chem. Ref. Data 2, 205
Lovas F.J., 1992, J. Phys. Chem. Ref. Data 21, 181
Liszt H, Lucas R., 1995, A&A 299, 847
Mangum J.G., Wootten A., Wadiak E.J., Loren R.B., 1990, ApJ 348, 542
Mangum J.G., Wootten A., 1993, ApJS 89, 123
Mauersberger R., Henkel C., 1989, A&A 223, 79
Mauersberger R., Henkel C., 1991, A&A 245, 457
Mauersberger R., Henkel C., 1993, Rev. Modern Astron. (Astronomische Gesellschaft) 6, 69
Mauersberger R., Henkel C., Chin Y.-N., 1995, A&A 294, 23
Mauersberger R., Henkel C., Wielebinski R., et al., 1996a, A&A, 305, 421
Mauersberger R., Henkel C., Whiteoak J.B., et al., 1996b, A&A 309, 705
McCall M.L., 1989, AJ 97, 1341
Menten K.M., 1987, Ph.D. Thesis, Bonn University

Menten K.M., Reid M.J., 1996, ApJ 465, L99
Menten K.M., Walmsley C.M., Henkel C., Wilson T.L., 1988, A&A 198, 267
Nakagawa N, 1980, in: Interstellar Molecules, ed. D.H. Andrew (D. Reidel Publishing Company, Dordrecht), p.365
Petuchowski S.J., Bennett C.L., 1992, ApJ 391, 137
Sastry K.V.N.L., Lees R.M., Van der Linde, J., 1981, J. Mol. Spectr. 88, 228
Seaquist E.R., Bell M.B., 1990, ApJ 364, 94
Shier L.M., Rieke M.J., Rieke G.H., 1994, ApJ 433, L9
Sinclair M.W., Carrad G.J., Caswell J.L., et al., 1992, MNRAS 256, 33P
Strong A.W., Bloemen J.B.G.M., Dame T.M., et al., 1988, A&A 207, 1
Takano S., Nakai N., Kawaguchi, K, 1995, PASJ 47, 801
Turner B.E., 1989, Space Sci. Rev. 51, 235
Turner, B.E., 1993, ApJ 410, 140
Walmsley C.M., Menten K.M., Batrla W., Matthews H.E., 1988, A&A 197, 271
Whiteoak J.B., Gardner F.F., 1976, MNRAS 174, 51P

This article was processed by the author using Springer-Verlag LaTeX A&A style file *L-AA* version 3.